



Fabrication of Kidney Proximal Tubule Grafts Using Biofunctionalized Electrospun Polymer Scaffolds

Katja Jansen, Miguel Castilho, Sanne Aarts, Michael M. Kaminski, Soeren S. Lienkamp, Roman Pichler, Jos Malda, Tina Vermonden, Jitske Jansen, and Rosalinde Masereeuw*

The increasing prevalence of end-stage renal disease and persistent shortage of donor organs call for alternative therapies for kidney patients. Dialysis remains an inferior treatment as clearance of large and protein-bound waste products depends on active tubular secretion. Biofabricated tissues could make a valuable contribution, but kidneys are highly intricate and multifunctional organs. Depending on the therapeutic objective, suitable cell sources and scaffolds must be selected. This study provides a proof-of-concept for stand-alone kidney tubule grafts with suitable mechanical properties for future implantation purposes. Porous tubular nanofiber scaffolds are fabricated by electrospinning 12%, 16%, and 20% poly- ϵ -caprolactone (PCL) v/w (chloroform and dimethylformamide, 1:3) around 0.7 mm needle templates. The resulting scaffolds consist of 92%, 69%, and 54% nanofibers compared to microfibers, respectively. After biofunctionalization with L-3,4-dihydroxyphenylalanine and collagen IV, 10×10^6 proximal tubule cells per mL are injected and cultured until experimental readout. A human-derived cell model can bridge all fiber-to-fiber distances to form a monolayer, whereas small-sized murine cells form monolayers on dense nanofiber meshes only. Fabricated constructs remain viable for at least 3 weeks and maintain functionality as shown by inhibitor-sensitive transport activity, which suggests clearance capacity for both negatively and positively charged solutes.


1. Introduction

Due to a constant scarcity of donor kidneys, approximately two million end-stage renal disease patients worldwide must undergo dialysis, which is the only treatment option besides organ transplantation. Unfortunately, hemodialysis does not provide the same long-term beneficial effects on quality of life and survival as kidney transplants, annual mortality of hemodialysis lies around 20%.^[1,2] This poor outcome is related to the therapeutic restrictions of dialysis: diffusion and convection remove only a fraction of metabolic waste products from the blood, predominantly small uremic solutes (<500 Da). Meanwhile, large and protein-bound solutes remain in the body as their clearance depends on active tubular secretion. Retention and gradual accumulation of the waste products, also known as uremic toxins, are a hallmark of chronic kidney disease (CKD) and are associated with disease progression, cardiovascular complications, and increased mortality.^[3]

K. Jansen, S. Aarts, Dr. T. Vermonden, Prof. R. Masereeuw
Division of Pharmacology
Utrecht Institute for Pharmaceutical Sciences
Utrecht University
Universiteitsweg 99, 3584 CG Utrecht, The Netherlands
E-mail: r.masereeuw@uu.nl

Dr. M. Castilho, S. Aarts, Prof. J. Malda
Department of Orthopaedics
University Medical Center Utrecht
Utrecht University
P.O. Box 85500, 3508 GA Utrecht, The Netherlands

Dr. J. Jansen
Department of Pathology and Pediatric Nephrology
RIMLS, RIHS
Radboud University Medical Center
P.O. Box 9101, 6500 HB Nijmegen, The Netherlands

 The ORCID identification number(s) for the author(s) of this article can be found under <https://doi.org/10.1002/mabi.201800412>.

Dr. T. Vermonden
Division of Pharmaceutics
Utrecht Institute for Pharmaceutical Sciences
Utrecht University
Universiteitsweg 99, 3584 CG Utrecht, The Netherlands

Dr. M. M. Kaminski, Dr. S. S. Lienkamp, Dr. R. Pichler
University Medical Center Freiburg
Zentrale Klinische Forschung
Breisacher Straße 66, 79106 Freiburg im Breisgau, Germany

Dr. M. Castilho, Prof. J. Malda, Dr. T. Vermonden, Prof. R. Masereeuw
Regenerative Medicine Center Utrecht
Uppsalalaan 8, 3584 CT Utrecht, The Netherlands

Prof. J. Malda
Department of Equine Sciences
Room G05228
University Medical Center Utrecht, Utrecht University
Heidelberglaan 100, 3584 CX Utrecht, The Netherlands

DOI: 10.1002/mabi.201800412

For this reason, renal assist devices (RADs) are being developed to enhance conventional dialysis. These devices include an extracorporeal cellular unit of renal proximal tubule epithelial cells, which express multiple transporters that cooperate in basolateral uptake and luminal excretion of various endogenous metabolites, including uremic toxins.^[3,4] FDA-approved phase I/II clinical studies with a RAD suggested a potential added value of such a device in the treatment of critically ill subjects.^[5–7] The development, current status, and technical challenges of RADs have been extensively reviewed elsewhere.^[2,8–10] Unfortunately, the efficiency of current RADs is limited to short-time extracorporeal applications. In the long run, implantable constructs for continuous blood clearance and maintained cell function would be the best solution.

Promising kidney engineering approaches comprise innovations from stem cell-based therapies and de novo organogenesis to kidney decellularization techniques and additive manufacturing technologies like 3D printing.^[11] Lab-grown functional and autologous transplants are the holy grail for overcoming donor kidney shortage, graft rejection, and lifelong immunosuppressive therapy. However, due to the immense anatomical and physiological complexity of the kidney, these approaches are still in their infancy and far from clinical application. To steer a middle course, we propose to downscale kidney engineering from a complex whole organ to implantable hollow tubes that follow the principle of RADs by taking advantage of the active secretion system of proximal tubule cells.

For the creation of kidney proximal tubules, recent approaches have mainly been focusing on the use of hydrogels.^[12–18] Although promising results have been obtained, these tubules are either intended for in vitro testing only, too fragile for transplantation, or embedded in bulk gels, which would hamper nutrient supply and clearance capacity if not adequately vascularized. Thus, other technologies are required for the fabrication of implantable kidney tubule constructs that display both high diffusibility and mechanical stability.

Solution electrospinning is a traditional method that has to date been employed to fabricate tubular poly- ϵ -caprolactone (PCL) scaffolds for vascular or neuronal grafts, which have proven biocompatibility and sufficient mechanical stability in mouse, dog, and sheep models.^[19–26] Electrospinning also enables the production of nanofiber scaffolds with high porosity and surface-to-volume ratio, which is essential for the desired diffusibility of bioengineered kidney tubes. Considering their excellent properties for high mechanical stability and diffusibility, electrospun nanofiber tubes would be superior to current hydrogel models for the creation of kidney proximal tubule grafts. Furthermore, biofunctionalized nanofiber meshes could mimic the micro-architecture of the native extracellular matrix (ECM), since the renal basement membrane mainly consists of cross-linked collagen IV fibers.^[27] By mimicking the macromolecular ECM architecture and composition as well as its stiffness, cell–ECM interactions could promote normal tissue homeostasis.^[28] Thus, electrospun nanofiber meshes have the potential to provide additional physicochemical cues for proper graft functionality.

The goal of this study was to electrospin porous tubular scaffolds that enable luminal epithelialization with proximal tubule epithelial cells to construct functional kidney tubule grafts. We electrospun 12%, 16%, and 20% v/w PCL (chloroform and

dimethylformamide, 1:3) scaffolds with distinct morphology and mechanical properties. After biofunctionalization with an L-3,4-dihydroxyphenylalanine (L-DOPA) and collagen IV double coating, we cultured two renal cell lines with different cell sizes and origin on the luminal scaffold surface and investigated tight junction formation, long-term viability, and transport functionality.

2. Results and Discussion

2.1. Scaffold Fabrication

In this study, we designed and characterized biofunctionalized polymer scaffolds for the fabrication of kidney proximal tubule grafts with a luminal tight monolayer of functional renal proximal tubule epithelial cells. An overview of the workflow is depicted in **Figure 1**.

We used 12%, 16%, and 20% v/w PCL dissolved in dimethylformamide and chloroform (ratio 3:1) to fabricate tubular nanofiber scaffolds, in the following referred to as 12%, 16%, and 20% PCL scaffolds. These scaffolds had an inner diameter of 0.7 mm, an outer diameter of approximately 1 mm, and distinct morphologies on microscale. The inner diameter was prespecified by the 0.7 mm needle template, which corresponds to around ten times the diameter of kidney tubules in situ. Although the physiological dimension might be technically feasible, it would have been impractical for experimental handling and is, aside from that, not a prerequisite for heterotrophic implantations. Key parameters of the electrospinning set-up, that is, electrical potential, spinneret-to-collector distance and feeding rate were optimized to obtain a stable electrified jet. Optimized settings were found with 9–17 kV, a feeding rate of 0.3–0.8 mL h⁻¹ for 20–30 min and a template distance of 7–12 cm. Using these settings, electrospinning of a 12% PCL solution resulted in stable tubular scaffolds with a wall thickness of $147 \pm 63 \mu\text{m}$ as compared to $298 \pm 107 \mu\text{m}$ for 16% and $247 \pm 90 \mu\text{m}$ for 20% PCL (**Figure 2a,b,d**). The wall thickness varied between but also within the scaffolds because of the nonuniform fiber organization, which is a typical characteristic of the electrospinning process. However, the fibers effectively distributed over the rotating needle template due to its electrostatic charge attraction and thereby tended toward an axial orientation pattern (**Figure 2c**). Also, the fiber diameter was slightly variable within each scaffold. With fiber diameters of 0.53 ± 0.30 , 0.88 ± 0.44 , and $1.06 \pm 0.66 \mu\text{m}$ for 12%, 16%, and 20% PCL scaffolds, respectively, the diameter increased significantly. Thereby, the percentage of nanofibers compared to microfibers dropped from 92% to 69% and 54%, respectively. It is worth noting that electrospinning of 12% PCL solutions resulted in the formation of beaded fibers, which are the typical consequence of too high surface tension and low polymer concentration or charge density. Beads are often considered a defect as their presence results in lower mechanical properties. However, this feature does not, per definition, hamper the use of 12% scaffolds for biological application.

In the current study, the demonstrated variations in wall and fiber thickness and hence limited reproducibility are considered a minor problem as we strived for a proof-of-concept for the fabrication of electrospun kidney tubule grafts with sufficient mechanical stability and maintained renal transport

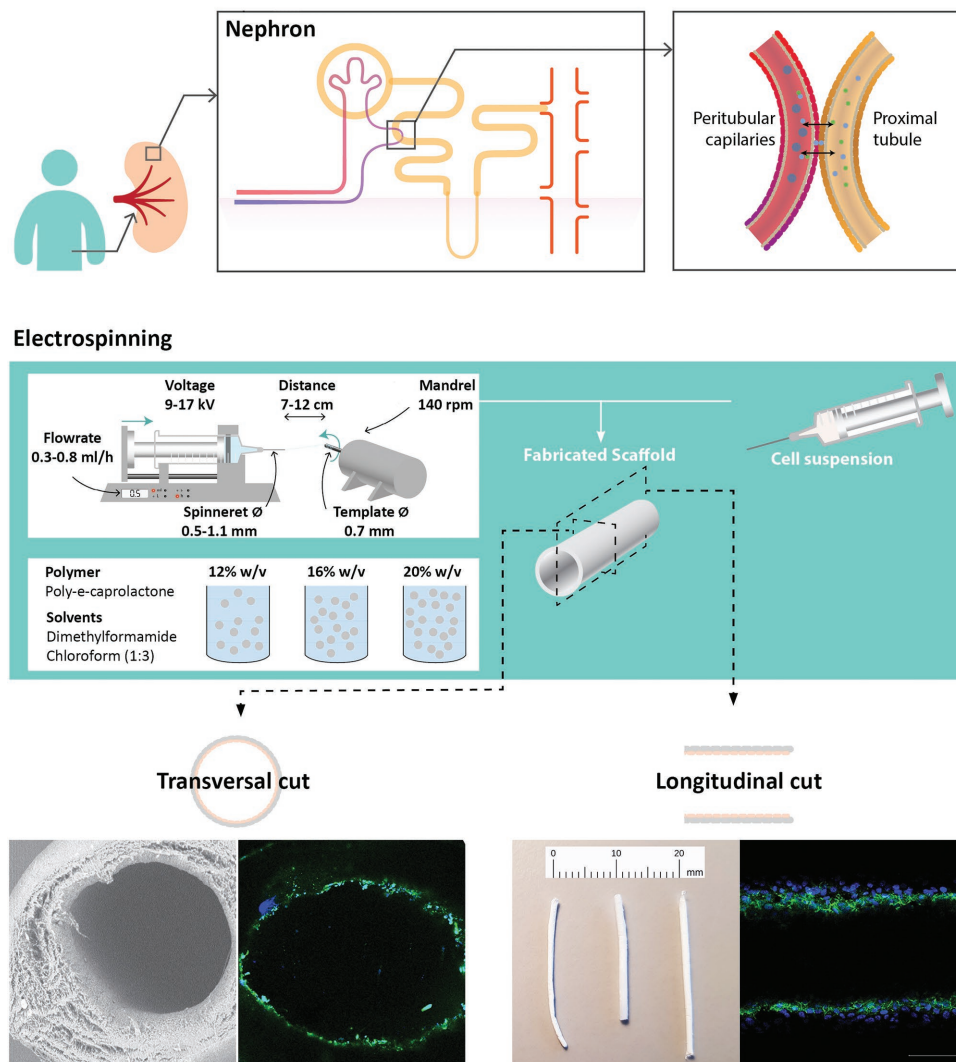


Figure 1. Workflow of design and fabrication of the biofunctionalized electrospun polymer scaffolds for kidney proximal tubule grafts. a) A kidney contains 200 000–1 000 000 functional units, the nephrons. After blood filtration through the glomerulus, active secretion of metabolic waste products takes place between the proximal tubules and peritubular capillaries. While filtration can be replaced by hemodialysis, active secretion requires proximal tubule cells as part of advanced renal replacement therapies. b) Solution electrospinning was used to fabricate tubular scaffolds with different polymer concentrations. Two cell lines of proximal tubular epithelial cells were injected for luminal epithelialization to construct implantable kidney tubule drafts. c) Scaffold properties and cell behavior were examined regarding mechanical properties, epithelialization, long-term viability, and renal functionality.

activity. Nonetheless, the production of scaffolds with well-defined wall thicknesses and fiber organization would be of future interest in order to comply to GMP guidelines as well as to obtain improved cell differentiation and function by providing a favorable microenvironment.^[29] To this end, the recently developed technology of melt electrospinning writing could advance the fabrication of tubular scaffolds with highly accurate fiber dispositions, but this falls beyond the scope of the current study.^[30,31]

2.2. Mechanical Scaffold Properties

After fabrication and structural characterization, the mechanical behavior of the tubular scaffolds was investigated under

uniaxial tensile loading (**Figure 3a,b**). An overall increase in tangent modulus as well as stress and strain at break was observed with increase in polymer concentration, which demonstrates increasing mechanical stability. The obtained tangent modulus of 20% PCL scaffolds with 67.7 ± 7.4 MPa was significantly higher than for 12% and 16% PCL scaffolds with 16.5 ± 7.6 and 23.5 ± 13.6 MPa, respectively (**Figure 3c**). Interestingly, the tangent moduli of 12% and 16% PCL scaffolds were comparable to the elasticity of native tubular basement membranes, for which values of 3–10 MPa have been reported.^[32] Furthermore, 16% and 20% PCL scaffolds exhibited a strain at break of at least 60%, which is a pivotal property, for example, to withstand fluid pressures and to resist the deformation required during implantation. The overall weaker mechanical properties of 12% PCL scaffolds can be

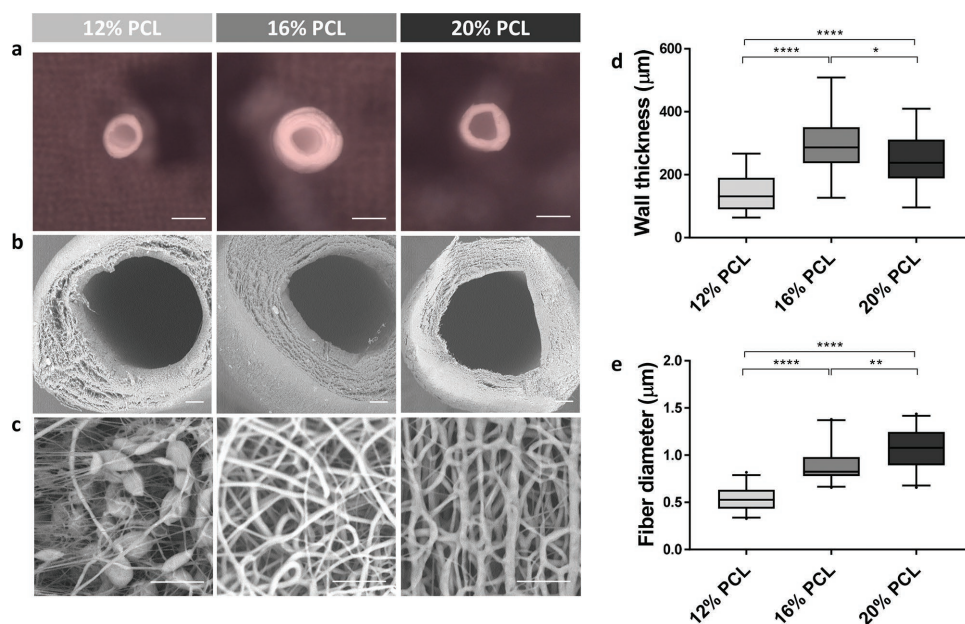


Figure 2. Scaffold fabrication. a–c) Scanning electron microscopic images of tubular electrospun scaffolds made of 12%, 16%, and 20% w/v PCL. Scale bars: (a) 1 mm and (b,c) 100 µm. d) Comparison of scaffold wall thicknesses, measured on four locations in three sections of three different scaffolds. e) Comparison of scaffold fiber diameters, measured on three locations in three sections of three different scaffolds. Boxplots present the mean and 5–95 percentiles. * $p < 0.05$, ** $p < 0.01$, *** $p < 0.0001$ using one-way ANOVA.

explained by the earlier reported presence of beaded fibers (Figure 2c).

2.3. Luminal Epithelialization

For epithelialization of the inner scaffold wall, two renal cell lines of different origin were used, of which the cells

considerably differed in cell size—induced renal tubular epithelial cells (iREC) were derived from murine fibroblasts through conversion into renal-like cells by transduction of essential transcription factors.^[33] For these cells, an average size of $13.7 \pm 1.3 \mu\text{m}$ was measured when cultured in PCL tubular scaffolds. Conditionally immortalized proximal tubule epithelial cells (ciPTEC) are urine-derived proximal tubule cells from human origin.^[34] In this study, we used a clonal cell line

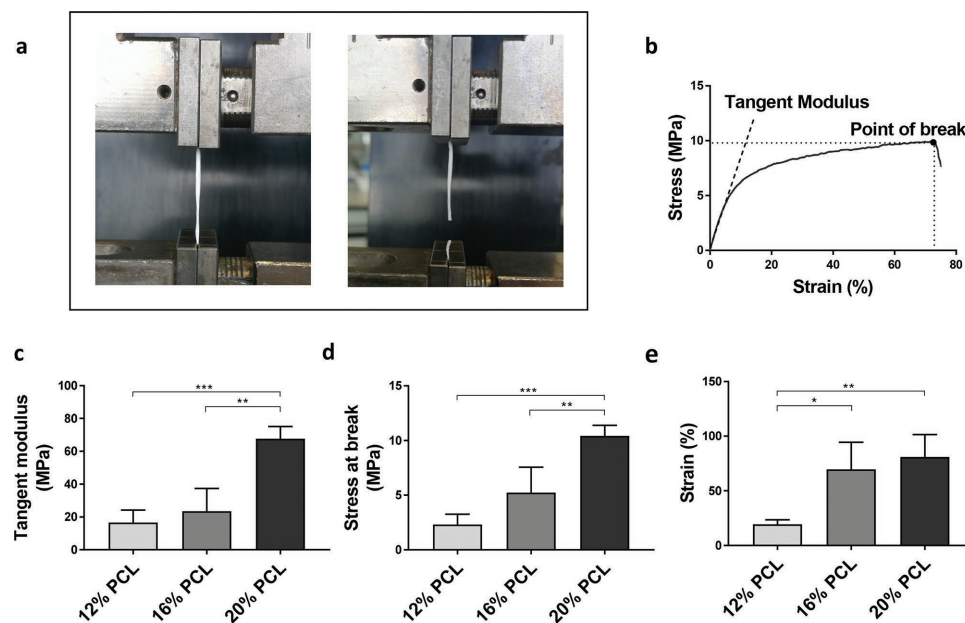


Figure 3. Mechanical scaffold properties. a) Experimental set-up for uniaxial tensile testing. b) Representative stress–strain curve for a 20% PCL scaffold with indicated tangent modulus and point at break. c) Comparison of tangent moduli ($n = 3$). d) Comparison of stress at break ($n = 3$). e) Comparison of strain at break ($n = 3$). Data are expressed as mean \pm SD. * $p < 0.05$, ** $p < 0.01$, *** $p < 0.001$ using one-way ANOVA.

transduced with Organic Anion Transporter 1 (OAT1), which has been proven to be functionally stable.^[35] The measured cell size of these cells was $29.7 \pm 5.5 \mu\text{m}$ when grown in PCL tubular scaffolds.

Due to the hydrophobic nature of PCL, cells were only partly able to adhere to the scaffolds, but adhesion properties were considerably improved by coating the PCL scaffolds with mussel-inspired adhesive L-DOPA and collagen IV, according to a method established previously.^[4,36–38] The double coating of L-DOPA and collagen IV enabled the formation of a complete and polarized epithelial monolayer (Figure 4a). Both cell lines were cultured on the luminal side of all three scaffolds and monolayer formation was investigated after 3 weeks (Figure 4b,c). Interestingly, iREC adhered to scaffolds of all three

polymer concentrations, but were only able to form a continuous intercellular barrier with high expression of the tight junction marker Zona Occludens 1 (ZO-1) on 12% PCL scaffolds, while ciPTEC were able to form tight monolayers on all three scaffolds. This indicates that the choice of polymer concentration for scaffold fabrication is not only critical for the desired mechanical properties of the scaffold, but also the resulting scaffold morphology has an essential impact on cell barrier formation, which is crucial to allow leakage-free and selective transport of solutes into the lumen. Here, the high content of nanofibers in 12% PCL scaffolds formed a sufficiently dense fiber mesh for the small-sized iREC to adhere and to form cell–cell contacts, whereas higher PCL concentrations created fiber-to-fiber distances that could only be bridged by the bigger-sized ciPTEC.

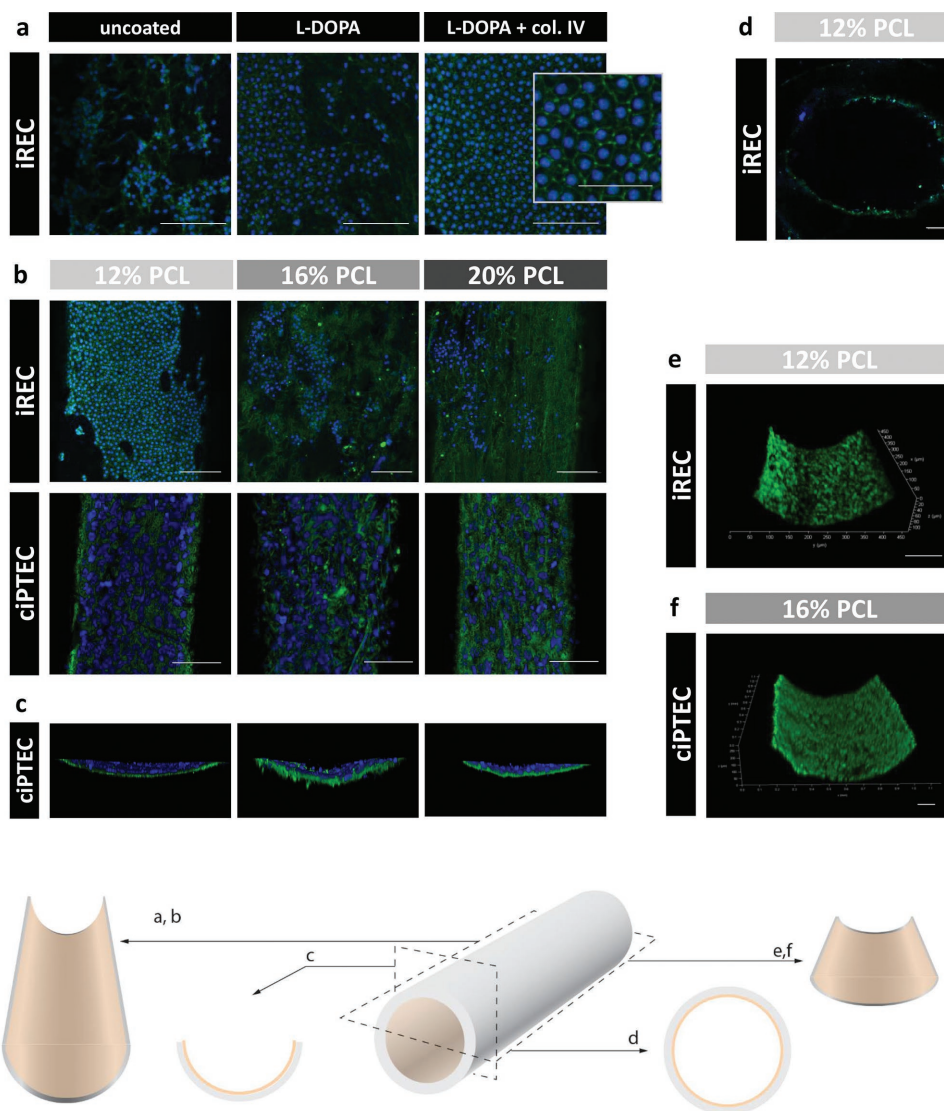


Figure 4. Luminal epithelialization. iREC or ciPTEC-OAT1 was cultured on the luminal side of 12%, 16%, and 20% w/v PCL scaffolds. a) Double coating with L-DOPA and collagen IV improved cell adhesion and tight monolayer formation as proven by visible tight junction marker zona occludens-1 (ZO-1, green) and nuclei (blue). b–c) iREC formed monolayers only on 12% PCL scaffolds. ciPTEC-OAT1 grew on all scaffolds into monolayers. In the absence of ZO-1, the scaffold fibers became visible due to autofluorescence. d) Transverse cut: cells grew throughout the scaffold lumen. e–f) Both cell lines showed high viability through enzymatic calcein-AM conversion to calcein (green) and absent staining with cell-impermeant viability indicator ethidium homodimer-1 (red). Scale bars: (a) 100 μm , 50 μm in the high magnification image.

A transverse scaffold view, as shown for ciPTEC (Figure 4c), and a transverse cut of a 12% PCL scaffold with iREC (Figure 4d) show that the cells formed luminal monolayers without significant migration into the scaffold and that the monolayers covered the entire scaffold surface. A viability assay confirmed the formation of dense and viable monolayers for both cell lines without any sign of material toxicity after at least 3 weeks of culture (Figure 4e,f).

2.4. Construct Functionality

For active uremic toxin removal, kidney proximal tubule grafts must not only possess a complete and tight monolayer, they must also be able to effectively transport metabolic solutes from the outside of the construct into the lumen for subsequent drainage. Renal proximal tubule epithelial cells possess a coordinated network of a multitude of transporters with overlapping specificities for the efficient transcellular transport of a broad spectrum of solutes. OAT1 and Organic Cation Transporter 2 (OCT2) are the most prominent basolateral transporters in human proximal tubule cells, which are responsible for the uptake of anionic and cationic metabolites, respectively. To demonstrate renal transport activity in our fabricated kidney proximal tubule grafts, 20% PCL scaffolds of matured ciPTEC were incubated for 10 min with the

fluorescent organic anion fluorescein or the fluorescent organic cation 4-(4-(Dimethylamino)-styryl)-*N*-methylpyridinium iodide (ASP⁺), in the absence or the presence of the OAT1 inhibitor probenecid or the OCT2 inhibitor tetrapentylammonium (TPA⁺). Fluorescence microscopy imaging confirmed substrate uptake with significant decrease in both fluorescein uptake ($p < 0.0001$) and ASP⁺ uptake ($p < 0.025$) in the presence of their respective transport protein inhibitor (Figure 5). These results suggest that electrospun tubular scaffolds allow the rapid diffusion of both negatively and positively charged compounds through the fibrous scaffold wall toward the basolateral side of the luminal cell monolayer. Moreover, we demonstrated that OAT1 and OCT2, both located at the basolateral membrane of tubular epithelial cells, maintained renal transport functionality for at least 3 weeks of culture. These are two very important features of kidney proximal tubule grafts for the efficient and continuous clearance of metabolic waste products from the body.

3. Conclusion

Tissue engineering is a rapidly developing field, but kidney engineering attempts to strive for a whole organ of yet inimitable complexity. Inspired by the principle of RADs, we down-scaled kidney engineering to simple tubular scaffolds with proximal tubule cells to focus on the unmet medical need of

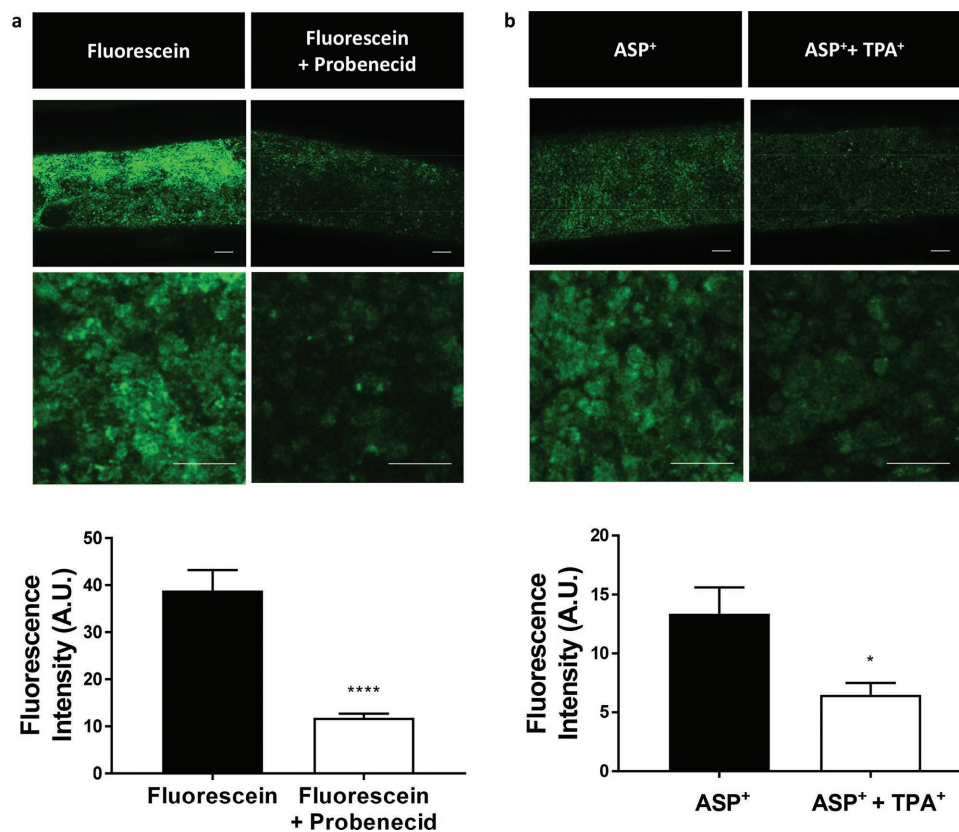


Figure 5. Cell functionality. ciPTEC-OAT1 cultured in 20% PCL scaffolds showed uptake of (left) 1 μM fluorescein via Organic Anion Transporter 1 (OAT1) and (right) 5 μM ASP⁺ via Organic Cation Transporter 2 (OCT2), which could be inhibited by 100 μM probenecid and 20 μM TPA⁺, respectively ($n = 5$). Scale bars: 100 μm. Data are expressed as mean ± SD. * $p < 0.05$, **** $p < 0.0001$ using Student's unpaired *t*-test.

active uremic toxin removal. Among the technologies used for the fabrication of porous tubular scaffolds, solution electrospinning is traditional and yet popular due to its simplicity and cost-effectiveness. Here, we demonstrated that biofunctionalized electrospun polymer scaffolds can be used for the creation of kidney proximal tubule grafts. Sufficient mechanical stability, rapid diffusibility, tight cellular monolayer formation, and prolonged construct viability and functionality demonstrated superior properties over existing proximal tubule models with regard to implantation purposes and continuous blood clearance as renal replacement therapy.

It should be noted that different cell sources must be developed and extensively characterized before implantation, for example, patient-derived or HLA-matching induced pluripotent stem cells that were differentiated to proximal tubule epithelial cells. Moreover, advanced biomaterials will likely further improve scaffold characteristics. For the first proof-of-concept of porous stand-alone kidney tubule grafts, we used PCL, a well-characterized biodegradable polymer, and a simple electrospinning set-up. However, scaffold fabrication should be extended to both more advanced materials, for example, collagen IV, hydrogel/scaffold composites, or decellularized extracellular matrices as well as more advanced technologies, for example, melt electrospinning writing. By selecting optimal parameters regarding scaffold dimensionality, topography, effective surface stiffness, and substrate thickness, we will be able to produce well-defined scaffolds with conceivably enhanced cell function.^[39–42] Thereby, advanced biofabrication approaches could enable the adaptation of RAD principles to implantable, well-defined tubular tissue constructs with fine-tuned mechanical properties and biological functionality.

4. Experimental Section

Preparation of Polymer Solutions: Poly-ε-caprolactone (PCL, midpoint 1.2 dL g⁻¹, Purasorb PC 12, Gorinchem, Netherlands) was dissolved 12%, 16%, or 20% w/v in chloroform and dimethylformamide in a ratio of 3:1. The polymer solution was mixed for at least 20 h.

Solution Electrospinning: An in-house built solution electrospinning setup was used in this study, as illustrated in Figure 1. The system consisted of a programmable syringe pump (NE-1000, New Era Pump Systems, Inc., USA) with a metallic syringe needle as spinneret, a brass tube as rotating collector equipped with a DC motor and a high voltage source (Heinzinger, LNC 1000–5 POS, 0–10 kV, Germany). Electrospun fibers were collected in the grounded rotating collector with a diameter of 0.7 mm positioned at 7–12 cm, opposite to the syringe pump. A rotation speed of approximately 140 rpm was fixed and kept for 20–30 min, while 12%, 16%, or 20% (w/v chloroform and dimethylformamide, 1:3) PCL solutions were electrospun with a feeding rate of 0.3–0.8 mL h⁻¹ and an applied voltage of 12–17 kV.

Mechanical Analysis: The mechanical behavior of the tubular constructs was tested under uniaxial tensile loading using a universal testing machine (Zwick Z010, Germany) equipped with a 1 kN load cell. Tests were performed at a rate of 1 mm min⁻¹. Prior to testing, the nominal dimensions of each sample, that is, diameter and length, were measured. The tangent modulus, strain, and stress at break were determined from the engineering stress–strain curves. Tangent moduli were calculated at the linear region (i.e., 2–5% strain region).

Scanning Electron Microscopic Imaging and Analysis: To analyze scaffold characteristics, images were captured with a Phenom desktop scanning electron microscope (Phenom world, Eindhoven, the Netherlands) at an acceleration speed of 10 kV. The samples were prepared by freezing three

scaffolds per PCL concentration in liquid nitrogen and three samples were cut: one section from the middle part of the scaffold and two from the outer ends. The wall thicknesses were measured at the top, left, right, and bottom of the section cuts. Fiber diameters were measured using 8000× magnified images in ImageJ (<https://imagej.net/Fiji/Downloads>). In each longitudinally opened sample, three locations were selected at the top, middle, and bottom. A line was drawn across the middle and the first 15 fibers that intersected this line were measured at the point of intersection, leading to a total of 45 measurements per sample and 135 per scaffold. For each scaffold, the ratio of micro- to nanofibers was calculated.

Scaffold Coating: Two milligrams per milliliter of L-3,4-dihydroxyphenylalanine (L-DOPA, Sigma–Aldrich, Zwijndrecht, the Netherlands) was dissolved in 10 mM Tris buffer at 37 °C for 45 min. After sterile filtration, scaffolds were coated with L-DOPA through submersion for 4 h at 37 °C with 90° turns every hour. After washing the scaffolds three times in Hank's Balanced Salt Solution (HBSS, Thermofisher Scientific, Bleiswijk, the Netherlands), 0.3 mg mL⁻¹ human collagen Bornstein and Traub Type IV (Sigma–Aldrich) was diluted 1:12 in HBSS, injected into the scaffold and incubated for 1 h at 37 °C. After the double coating, scaffolds were rinsed and kept in HBSS for 24 h before cell seeding. Coating materials, concentrations, and incubation times have been determined and optimized for renal cell culture by previous studies.^[4,36]

Cell Culture: Conditionally immortalized proximal tubule epithelial cells (ciPTEC) were developed by Wilmer et al. through infection with temperature-sensitive mutant U19tsA58 of SV40 large T antigen (SV40T) and the essential catalytic subunit of human telomerase (hTERT), and further transduced with the henceforth constitutively expressed OAT1 by Nieskens et al.^[34,35] To maintain a cell proliferation state, ciPTEC-OAT1 were cultured at 33 °C and 5% v/v CO₂, up to 90% confluency in T175 culture flasks (Greiner Bio-One, Alphen aan den Rijn, the Netherlands) using Dulbecco's modified eagle medium/HAM's F12 (Thermofisher Scientific), supplemented with 5 μg mL⁻¹ insulin, 5 μg mL⁻¹ transferrin, 5 μg mL⁻¹ selenium, 35 ng mL⁻¹ hydrocortisone, 10 ng mL⁻¹ epidermal growth factor, 40 pg mL⁻¹ tri-iodothyronine (Sigma–Aldrich), 10% fetal bovine serum (FBS, Greiner Bio-One), and 1% penicillin/streptomycin (Thermofisher Scientific). For cell maturation, ciPTEC-OAT1 were transferred to 37 °C for 7 days prior to experimental readout with omission of penicillin/streptomycin.

Induced renal tubular epithelial cells (iREC) were developed by Kaminski et al. by directly reprogramming mouse fibroblasts into renal-like cells through transfection of the transcription factors Emx2, Hnf1b, Hnf4a, and Pax8.^[33] Cells were cultured in Dulbecco's modified Eagle's medium (DMEM) supplemented with 10% FBS and 1% penicillin/streptomycin. The latter was omitted 7 days prior to experimental readout.

Cell Culture in Biofunctionalized PCL Scaffolds: Immediately after electrospinning, tubular scaffolds were first sterilized using 365 nm UV light (2.6 mW cm⁻², UVP CL-1000) on both sides for 15 min each. Subsequently, the constructs were injected twice with 10 × 10⁶ cells per mL followed by 2 h incubations at 33 °C (ciPTEC-OAT1) or 37 °C (iREC) in dry 12-well plates with a 180° turn in between, before culture medium was added. The following day, the scaffolds were transferred into new 12-well plates and cultured for 3 weeks.

Immunofluorescence: Matured ciPTEC and iREC were fixed with 2% w/v paraformaldehyde in HBSS and permeabilized with 0.3% v/v triton X-100 in HBSS for 10 min. To prevent nonspecific antibody-binding, the cells were exposed to a block solution consisting of 2% v/v FCS, 2% v/v bovine serum albumin (BSA), and 0.1% v/v tween-20 in HBSS for 30 min. The primary antibody against the tight junction protein zonula occludens 1 (ZO-1, Thermofisher Scientific) was diluted 1:50 in block solution and the cells were incubated for 1 h, followed by incubation with goat-anti-rabbit-Alexa488 conjugate (1:200, Life Technologies Europe BV, Bleiswijk, The Netherlands) for 30 min. Finally, nuclei were stained using DAPI nuclei staining (Sigma–Aldrich, 1:1000) for 7 min and the scaffolds were mounted with Prolong Antifade Mounting Medium (Thermofisher Scientific) in Willco wells glass bottom dishes (WillCo Wells BV,



Amsterdam, the Netherlands). ZO-1 expression and localization were examined using the confocal microscope Leica TCS SP8 X, filters of 410–494 nm and 512–551 nm, and software Leica Application Suite X.

Live/Dead Viability Assay: To determine cell viability/cytotoxicity after 3 weeks of cell culture in tubular PCL scaffolds, the scaffolds were rinsed in HBSS and incubated with 2 μM calcein-AM and 1 μM ethidium homodimer-1 (ThermoFisher Scientific) for 15 min at 37 °C. Images were captured with filters set at 544–572 nm and 625–686 nm, using the confocal microscope Leica TCS SP8 X and software Leica Application Suite X.

Transport Assays: To test transport functionality after 3 weeks of cell culture, five 20% PCL scaffolds with cPTEC-OAT1 were rinsed in HBSS and incubated with 1 μM fluorescent OAT1 substrate fluorescein in the presence or the absence of 100 μM OAT1 inhibitor probenecid for 10 min at 37 °C. Another five scaffolds were incubated with 5 μM of the OCT2 substrate 4-(4-(dimethylamino)-styryl)-N-methylpyridinium iodide (ASP⁺) in the presence or the absence of 20 μM OCT2 inhibitor tetrapentylammonium (TPA⁺) for 10 min at 37 °C. After incubation, the scaffolds were rinsed in ice-cold HBSS, cut open longitudinally, and images were captured at 520–600 nm using the confocal microscope Leica TCS SP8 X and software Leica Application Suite X. Fluorescence intensity was semi-quantified using ImageJ with 16 bit images and background subtraction.

Data Analysis: Unless stated otherwise, a minimum of three scaffolds of each polymer concentration was used per experiment. Data were analyzed in Graphpad Prism 7 (GraphPad Software Inc., La Jolla, USA) using Student's unpaired *t*-test or one-way ANOVA with multiple comparisons.

Acknowledgements

This study was financed by the Netherlands Organisation for Scientific Research (NWO) as part of the “Future Medicines” Research Program (022.006.003) and by the Strategic Alliance University Medical Center Utrecht–Technical University Eindhoven, the European Research Council (ERC) (consolidator Grant 3D-JOINT, (#647426)). The authors would like to thank J. H. van Duijn for technical assistance with the solution electrospinning device.

Conflict of Interest

The authors declare no conflict of interest.

Keywords

polycaprolactone, regenerative medicine, renal replacement therapy, renal transport, tissue engineering

Received: October 25, 2018
Published online: December 13, 2018

- [1] J. Galliford, D. S. Game, *Postgrad. Med. J.* **2009**, *85*, 91.
- [2] S. Kim, W. H. Fissell, D. H. Humes, S. Roy, *Front. Biosci., Elite Ed.* **2015**, *7*, 215.
- [3] R. Masereeuw, H. A. Mutsaers, T. Toyohara, T. Abe, S. Jhawar, D. H. Sweet, J. Lowenstein, *Semin. Nephrol.* **2014**, *34*, 191.
- [4] J. Jansen, I. E. De Napoli, M. Fedecostante, C. M. Schophuizen, N. V. Chevchik, M. J. Wilmer, A. H. van Asbeck, H. J. Croes, J. C. Pertijs, J. F. Wetzels, L. B. Hilbrands, L. P. van den Heuvel, J. G. Hoenderop, D. Stamatialis, R. Masereeuw, *Sci. Rep.* **2015**, *5*, 16702.
- [5] J. Tumlin, R. Wali, W. Williams, P. Murray, A. J. Tolwani, A. K. Vinnikova, H. M. Szerlip, J. Ye, E. P. Paganini, L. Dworkin, K. W. Finkel, M. A. Kraus, H. D. Humes, *J. Am. Soc. Nephrol.* **2008**, *19*, 1034.
- [6] J. A. Tumlin, C. M. Galphin, A. J. Tolwani, M. R. Chan, A. Vijayan, K. Finkel, B. Szamosfalvi, D. Dev, J. R. DaSilva, B. C. Astor, A. S. Yevzlin, H. D. Humes, SCD Investigator Group, *PLoS One* **2015**, *10*, e0132482.
- [7] K. A. Johnston, A. J. Westover, A. Rojas-Pena, D. A. Buffington, C. J. Pino, P. L. Smith, H. D. Humes, *J. Tissue Eng. Regen. Med.* **2017**, *11*, 3048.
- [8] J. Jansen, M. Fedecostante, M. J. Wilmer, L. P. van den Heuvel, J. G. Hoenderop, R. Masereeuw, *Biotechnol. Adv.* **2014**, *32*, 1317.
- [9] J. H. Song, H. D. Humes, *Curr. Drug Targets* **2009**, *10*, 1227.
- [10] M. K. van Gelder, S. M. Mihaila, J. Jansen, M. Wester, M. C. Verhaar, J. A. Joles, D. Stamatialis, R. Masereeuw, K. G. F. Gerritsen, *Expert Rev. Med. Devices* **2018**, *15*, 323.
- [11] A. Peloso, R. Katari, S. V. Murphy, J. P. Zambon, A. DeFrancesco, A. C. Farney, J. Rogers, R. J. Stratta, T. M. Manzia, G. Orlando, *Expert Opin. Biol. Ther.* **2015**, *15*, 547.
- [12] J. Vriend, T. T. G. Nieskens, M. K. Vormann, B. T. van den Berge, A. van den Heuvel, F. G. M. Russel, L. Suter-Dick, H. L. Lanz, P. Vulto, R. Masereeuw, M. J. Wilmer, *AAPS J.* **2018**, *20*, 87.
- [13] M. Hu, M. Kurisawa, R. Deng, C. M. Teo, A. Schumacher, Y. X. Thong, L. Wang, K. M. Schumacher, J. Y. Ying, *Biomaterials* **2009**, *30*, 3523.
- [14] C. Shen, G. Zhang, Q. Wang, Q. Meng, *ACS Appl. Mater. Interfaces* **2015**, *7*, 19789.
- [15] K. A. Homan, D. B. Kolesky, M. A. Skylar-Scott, J. Herrmann, H. Obuobi, A. Moisan, J. A. Lewis, *Sci. Rep.* **2016**, *6*, 34845.
- [16] S. H. Lu, Q. Lin, Y. N. Liu, Q. Gao, T. Hao, Y. Wang, J. Zhou, H. Wang, Z. Du, J. Wu, C. Y. Wang, *J. Tissue Eng. Regen. Med.* **2012**, *6*, 786.
- [17] E. J. Weber, A. Chapron, B. D. Chapron, J. L. Voellinger, K. A. Lidberg, C. K. Yeung, Z. Wang, Y. Yamaura, D. W. Hailey, T. Neumann, D. D. Shen, K. E. Thummel, K. A. Muczynski, J. Himmelfarb, E. J. Kelly, *Kidney Int.* **2016**, *90*, 627.
- [18] K. Jansen, C. C. L. Schuurmans, J. Jansen, R. Masereeuw, T. Vermonden, *Curr. Pharm. Des.* **2017**, *23*, 3845.
- [19] M. Zhou, W. Qiao, Z. Liu, T. Shang, T. Qiao, C. Mao, C. Liu, *Tissue Eng., Part A* **2014**, *20*, 79.
- [20] Y. Qiu, N. Zhang, Q. Kang, Y. An, X. Wen, *J. Biomed. Mater. Res., Part B* **2009**, *90B*, 668.
- [21] H. Wang, Y. Feng, H. Zhao, Z. Fang, M. Khan, J. Guo, *J. Nanosci. Nanotechnol.* **2013**, *13*, 1578.
- [22] A. Wang, Q. Ao, W. Cao, M. Yu, Q. He, L. Kong, L. Zhang, Y. Gong, X. Zhang, *J. Biomed. Mater. Res., Part A* **2006**, *79A*, 36.
- [23] C. Huang, R. Chen, Q. Ke, Y. Morsi, K. Zhang, X. Mo, *Colloids Surf., B* **2011**, *82*, 307.
- [24] S. Wang, X. M. Mo, B. J. Jiang, C. J. Gao, H. S. Wang, Y. G. Zhuang, L. J. Qiu, *Int. J. Nanomed.* **2013**, *8*, 2131.
- [25] T. Fukunishi, C. A. Best, T. Sugiura, T. Shoji, T. Yi, B. Udelsman, D. Ohst, C. S. Ong, H. Zhang, T. Shinoka, C. K. Breuer, J. Johnson, N. Hibino, *PLoS One* **2016**, *11*, e0158555.
- [26] Y. Li, K. Jiang, J. Feng, J. Liu, R. Huang, Z. Chen, J. Yang, Z. Dai, Y. Chen, N. Wang, W. Zhang, W. Zheng, G. Yang, X. Jiang, *Adv. Healthcare Mater.* **2017**, *6*, 1601343.
- [27] A. M. van Genderen, J. Jansen, C. Cheng, T. Vermonden, R. Masereeuw, *Adv. Healthcare Mater.* **2018**, *7*, 1800529.
- [28] C. M. Borza, X. Chen, R. Zent, A. Pozzi, *Curr. Top. Membr.* **2015**, *76*, 231.
- [29] C. Liu, C. Zhu, J. Li, P. Zhou, M. Chen, H. Yang, B. Li, *Bone Res.* **2015**, *3*, 15012.
- [30] F. M. Wunner, O. Bas, N. T. Saidy, P. D. Dalton, E. M. D. Pardo, D. W. Huttmacher, *J. Visualized Exp.* **2017**, *130*, e56289.
- [31] M. Castilho, D. Feyen, M. Flandes-Iparraguirre, G. Hochleitner, J. Groll, P. A. F. Doevendans, T. Vermonden, K. Ito, J. P. G. Sluijter, J. Malda, *Adv. Healthcare Mater.* **2017**, *6*, 1700311.

- [32] A. M. van Genderen, J. Jansen, C. Cheng, T. Vermonden, R. Masereeuw, *Adv. Healthcare Mater.* **2018**, *7*, 1800529.
- [33] M. M. Kaminski, J. Tomic, C. Kresbach, H. Engel, J. Klockenbusch, A. L. Muller, R. Pichler, F. Grahmmer, O. Kretz, T. B. Huber, G. Walz, S. J. Arnold, S. S. Lienkamp, *Nat. Cell Biol.* **2016**, *18*, 1269.
- [34] M. J. Wilmer, M. A. Saleem, R. Masereeuw, L. Ni, T. J. van der Velden, F. G. Russel, P. W. Mathieson, L. A. Monnens, L. P. van den Heuvel, E. N. Levtchenko, *Cell Tissue Res.* **2010**, *339*, 449.
- [35] T. T. Nieskens, J. G. Peters, M. J. Schreurs, N. Smits, R. Woestenenk, K. Jansen, T. K. van der Made, M. Roring, C. Hilgendorf, M. J. Wilmer, R. Masereeuw, *AAPS J.* **2016**, *18*, 465.
- [36] C. M. Schophuizen, I. E. De Napoli, J. Jansen, S. Teixeira, M. J. Wilmer, J. G. Hoenderop, L. P. Van den Heuvel, R. Masereeuw, D. Stamatialis, *Acta Biomater.* **2015**, *14*, 22.
- [37] M. Ni, J. C. Teo, M. S. Ibrahim, K. Zhang, F. Tasnim, P. Y. Chow, D. Zink, J. Y. Ying, *Biomaterials* **2011**, *32*, 1465.
- [38] N. V. Chevtchik, M. Fedecostante, J. Jansen, M. Mihajlovic, M. Wilmer, M. Ruth, R. Masereeuw, D. Stamatialis, *Eur. J. Pharmacol.* **2016**, *790*, 28.
- [39] J. Visser, F. P. Melchels, J. E. Jeon, E. M. van Bussel, L. S. Kimpton, H. M. Byrne, W. J. Dhert, P. D. Dalton, D. W. Hutmacher, J. Malda, *Nat. Commun.* **2015**, *6*, 6933.
- [40] C. Dhand, Y. Balakrishnan, S. T. Ong, N. Dwivedi, J. R. Venugopal, S. Harini, C. M. Leung, K. Z. W. Low, X. J. Loh, R. W. Beuerman, S. Ramakrishna, N. K. Verma, R. Lakshminarayanan, *Int. J. Nanomed.* **2018**, *13*, 4473.
- [41] T. H. Kim, Y. Jung, S. H. Kim, *Tissue Eng., Part A* **2018**, *24*, 830.
- [42] C. H. Feng, Y. C. Cheng, P. H. Chao, *Acta Biomater.* **2013**, *9*, 5502.